Kaon electroproduction on ^{2}H and ^{3}He

Mikhail Egorov
Physics Faculty, Tomsk State University, Tomsk 634050, Russia

(Received 1 July 2022; revised 27 August 2022; accepted 23 December 2022; published 18 January 2023)

Differential and total cross sections for the reactions $^2\mathrm{H}(\gamma, K^0\Lambda)\,^1\mathrm{H}$, $^2\mathrm{H}(\gamma, K^+\Lambda)n$, $^2\mathrm{H}(\gamma, K^+\Sigma^0)n$, $^2\mathrm{H}(\gamma, K^+\Sigma^-)\,^1\mathrm{H}$, $^3\mathrm{He}(\gamma_V, K^+)^3_\Lambda\mathrm{H}$, and $^3\mathrm{He}(\gamma_V, K^+\Lambda)X$ taking into account the effects of KN, $K\Lambda$, and $N\Lambda$ interactions in the final state are presented. A comparison with the few experimental data on kaon photoproduction on the deuteron and on kaon electroproduction on ^{2}H and ^{3}He at $W_N = 1.91$ GeV, $Q^2 = 0.35$ GeV^2 is made. It is shown that the presented model correctly reproduces the dependence of the cross sections on energies and angles, especially in the region of small kaon emission angles. The eigenfunctions of the nuclei ^{3}He and $^3_\Lambda$H are directly obtained in this work by solving coupled homogeneous Faddeev equations with respect to the components of a three-body T matrix. The cross sections of $^3\mathrm{He}(\gamma_V, K^+)^3_\Lambda\mathrm{H}$ and $^3\mathrm{He}(\gamma_V, K^+\Lambda)X$ with these functions are calculated, and results also turned out to be in good agreement with the available experimental data. An analysis of the calculated cross sections for kaon photo- and electroproduction on the ^{3}He nucleus showed that the magnitude of the final state interaction effects in the considered processes is negligible, noticeable only in the region of large kaon emission angles.

DOI: 10.1103/PhysRevC.107.014611

I. INTRODUCTION

Electromagnetic production of $s\bar{s}$ quark pairs in a nuclei allows one to better understand the dynamics of strange hadrons, shedding light on the magnitude of the hyperon-nucleon interaction in the nuclear medium and on the contribution of the interaction of kaons and hyperons with nucleons in the final state. In addition, photoproduction of neutral kaons on a deuteron in the absence of neutron targets allows for more accurate identification of the position and parameters of baryon resonances. In this case, for the process $^2\mathrm{H}(\gamma, K^0\Lambda)\,^1\mathrm{H}$ the amplitude contains only the neutron part with a small admixture of proton, which is contained in the part responsible for the final state interaction.

The first measurements of the differential and total cross section of the reaction $^2\mathrm{H}(\gamma, K^0\Lambda)\,^1\mathrm{H}$ were performed on the CLAS [1] detector in the Thomas Jefferson National Accelerator Facility laboratory. The isobar model KaonMAID [2] and fit [3] were used to describe the experimental data obtained in [1] and to clarify the contribution of s-channel N^* resonances to the cross section of kaon photoproduction.

The experimental study of K^+ electroproduction on helium was performed only in the work [4] in coherent processes of Λ-hypernuclei production and in the work [5] in quasifree processes of kaon production in $K^+\Lambda$, $K^+\Sigma^0$, and $K^+\Sigma^-$ channels. The work [4] shows qualitative agreement with the experiment of theoretical ratios $\sigma_{\mathrm{lab}}(^{3,4}\mathrm{He})/\sigma_{\mathrm{lab}}(^1\mathrm{H})$ of the laboratory cross sections of $^{3,4}\mathrm{He}(e, e'K^+)^{3,4}_\Lambda\mathrm{H}$ to the cross section on the free proton. The values $\sigma_{\mathrm{lab}}(^{3,4}\mathrm{He})$ have been calculated with the use of model nuclear form factors [6]. An estimation of final state interaction of Λ hyperons with nucleons on ^{3,4}He targets in the region of small kaon emission angles in the laboratory frame was carried out in work [5] using the NSC97f hyperon-nucleon potential and amounted to 7–15% of cross section. A theoretical evaluation of the final state interaction of a Λ hyperon with nucleons in the process $^3\mathrm{He}(\gamma_V, K^+\Lambda)X$ was earlier carried out in [7] using a separable ΛN potential. It has been shown that the ΛN interaction can be significant in the region of small kaon emission angles. No other microscopic calculations of the interaction of kaons, hyperons, and nucleons in the final state of electromagnetic production of kaons on nuclei have been carried out.

Another question is the extent to which the known wave functions of light nuclei adequately reproduce their internal structure in the processes of kaon electroproduction in the region of large momentum transfer. The strong influence of the wave functions of ^{3}He, $^3_\Lambda$H on the cross section of kaon electro- and photoproduction was already noted earlier in [8]. The work showed that only with the placement of a final hyperon on the mass shell can the theory be reconciled with the experiment of [4]. No other studies of the influence of wave functions of hypernuclei in the processes of photo- and electroproduction of kaons on light nuclei have been carried out. The processes (γ, π) also provide an opportunity to test the known three-body wave functions of involved three-body nuclei in a wide range of transferred momenta, and also provide a serious check for elementary production operators. The latest data on $^3\mathrm{He}(\gamma, \pi^+)\,^3\mathrm{H}$ process [9] in the region of photon energies 0.5–1.55 GeV indicate the need to find additional contributions to the already known two-body corrections [10], which are absent in the impulse approximation, and which begin to play a significant role in the region $E_\gamma > 0.5$ GeV, $\theta_\pi > 60^\circ$. Such two-body corrections to the impulse approximation, which, along with the use of Faddeev's three-body function,

improve the agreement of the theory with experiment only in the region of large momentum transfer in the backward hemisphere of pion emission angles, should compensate for the lack (if it exists) of an accurate calculation of the three-body function in the same kinematic region. Models of processes $^3\mathrm{He}(\gamma,\pi)$, also including the various corrections to the impulse approximation, have previously encountered problems in describing experimental data both in the area of small pion emission angles [11,12], and at fixed momentum transfer [13]. Accurate treatment of the ^{3}He internal structure is necessary not only in the pion photo- and electroproduction, but also in the electromagnetic production of η mesons [14–16], in which the η-nuclear final state interaction in the threshold area is highly important. To date, no microscopic model adequately reproduces the cross section of coherent photoproduction of η mesons on the ^{3}He nucleus, especially above the breakup threshold. Therefore, there is no doubt that accurate treatment of nuclear wave functions in processes characterized by high momentum transfer is necessary for the study of meson photo- and electroproduction on light nuclei.

In this paper, systematic calculations of the cross sections of kaon photo- and electroproduction on ^{2}H and ^{3}He nuclei are carried out using a widely proven elementary production operator and with precise consideration of the interaction of kaons and hyperons with nucleons in the final state. In this work, further steps are also taken to obtain and analyze the microscopic wave functions of three-body systems ^{3}He and $^3_\Lambda$H. Section II is devoted to the formalism used in photo- and electroproduction of kaons on light nuclei. Section III describes the procedure for searching for three-body wave functions which were used in calculations. Section IV describes the procedure for accounting for interaction in the final state. The main results and discussion of the work are given in Sec. V.

II. FORMALISM

The interaction of a virtual photon γ_V with a proton and a neutron is characterized by three different isotopic channels of kaon photo- and electroproduction. Using standard kinematic variables for the energies ω_γ (photon), E_N (initial nucleon), E_K (kaon), and E_Y (hyperon) and for the momenta $\vec{k}$ (photon) and $\vec{q}$ (kaon) in the overall center-of-mass system (CMS), one has the following types of considered electroproduction processes on a proton:

$$\gamma_V(\omega_\gamma,\vec{k})+p(E_N,-\vec{k}) \to \begin{cases} K^+(E_K,\vec{q})+\Lambda(E_Y,-\vec{q}) & (1,0), \\ K^+(E_K,\vec{q})+\Sigma^0(E_Y,-\vec{q}) & \left(\frac{1}{\sqrt{3}},\frac{2}{3}\right), \\ K^0(E_K,\vec{q})+\Sigma^+(E_Y,-\vec{q}) & \left(-\sqrt{\frac{2}{3}},\frac{\sqrt{2}}{3}\right); \end{cases} \tag{1}$$

and on a neutron:

$$\gamma_V(\omega_\gamma,\vec{k})+n(E_N,-\vec{k}) \to \begin{cases} K^0(E_K,\vec{q})+\Lambda(E_Y,-\vec{q}) & (1,0), \\ K^0(E_K,\vec{q})+\Sigma^0(E_Y,-\vec{q}) & \left(-\frac{1}{\sqrt{3}},\frac{2}{3}\right), \\ K^+(E_K,\vec{q})+\Sigma^-(E_Y,-\vec{q}) & \left(\sqrt{\frac{2}{3}},\frac{\sqrt{2}}{3}\right). \end{cases} \tag{2}$$

The isospins multipliers are indicated in parentheses, ($T=1/2$, $T=3/2$), separately for channels with intermediate isospins $T=1/2$ and $T=3/2$. For kaon electroproduction, not only the energy dependence of $\omega_\gamma(Q^2)$ on Q^2 momentum transfer of the γ_V photon plays an essential role; so does the contribution of the longitudinal photon couplings (with nonzero contribution of $\epsilon_0=\epsilon_z=+1$ component of virtual-photon polarization vector $\vec{\epsilon}$) to the total amplitude of the processes (1) and (2). The photo- and electroproduction elementary operator for (1) and (2) has a general form in the matrix representation,

$$\langle Y,K|\hat{t}(Q^2,W_N,\vec{k},\vec{q})|N,\gamma\rangle=(-1)^{\bar{m}_s}i^{\bar{s}}C^{\frac{1}{2}m_{s'}}_{\frac{1}{2}m_s\,\bar{s}-\bar{m}_s}(K^{[\bar{s}][\bar{t}]})_{\bar{m}_s}. \tag{3}$$

In (3), notation is used for the Klebsch-Gordan coefficients connecting spin (1/2) and its projection m_s of the initial nucleon with spin (1/2) and its projection $m_{s'}$ of the final hyperon. Tensor $K^{[\bar{s}][\bar{t}]}$ determines the contributions of the isoscalar ($\bar{t}=0$) and isovector ($\bar{t}=1$) components of the elementary amplitude, as well as the non-spin-flip ($\bar{s}=0$) and spin-flip ($\bar{s}=1$) its parts. For comparison with the data from [1], it is necessary to take the single-nucleon total energy W_N as an independent quantity associated with the total energy of the system W and the photon energy ω_γ in the CMS by the following relations:

$$E_\gamma=\frac{W_N^2-M_N^2}{2M_N},\quad W=\sqrt{M_A(M_A+2E_\gamma)},$$
$$\omega_\gamma=\frac{W^2-Q^2-M_A^2}{2W}. \tag{4}$$

The mass of the target nucleus in (4) is denoted as M_A. The isotopic structure of the tensor $K^{[\bar{s}][\bar{t}]}$ for the processes (1) and (2) is the sum of the isoscalar and isovector amplitudes,

$$K^{[\bar{s}][\bar{t}]}=(K^{[\bar{s}][\bar{t}=0]}+(-1)^bK^{[\bar{s}][\bar{t}=1]}), \tag{5}$$

the signs of which are determined by the following rule: $b=0$ for processes (1) and $b=1$ for processes (2). Thus, to determine the nuclear amplitude, one should as the sum of the contributions $K^{[\bar{s}][\bar{t}=0]}$ and $K^{[\bar{s}][\bar{t}=1]}$, like as their difference for each of the six charge channels.

In this work, the model of kaon photo- and electroproduction on a proton [17] is used, which allows one to find only the sum of the contributions of the isoscalar and isovector amplitudes (5). A characteristic feature of the $N(\gamma,KY)$ model used is the relatively strong suppression of background Born terms, as a result of which the main contribution to the cross section is associated with the excitation of baryon resonances. For kaon photo- and electroproduction, the parameters of hadron resonances were fixed in [17] from the visible agreement of the calculated total and differential cross sections with available experimental data in three charge channels, $K^+\Lambda$, $K^+\Sigma^0$, and $K^0\Sigma^+$. A characteristic feature of the model [17] is the use of sufficiently strong, Q^2-dependent form factors for suppressing background terms of the single-nucleon amplitude. The longitudinal components of the amplitude of the kaon electroproduction which depend on ϵ_0 are also strongly damped by form factors. In this model gauge invariance is in order of resonance terms

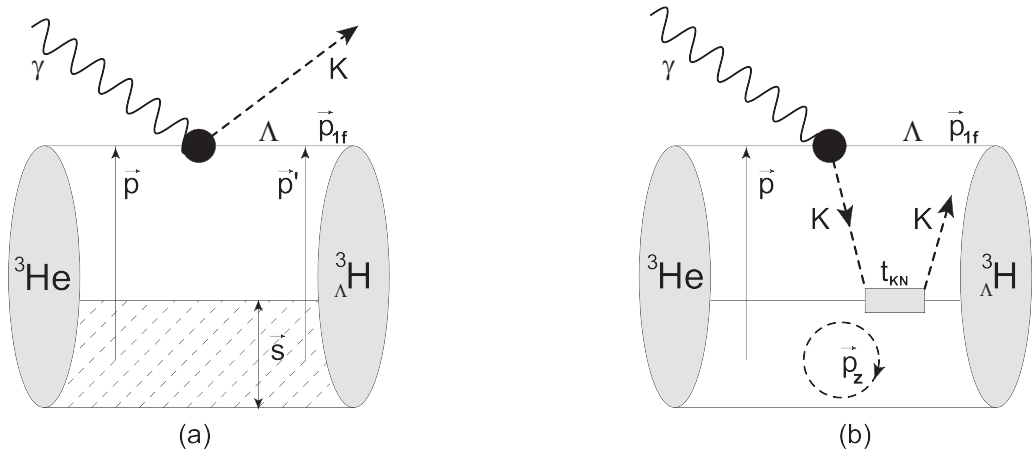

FIG. 1. Schematic illustration of the coherent process $^3\mathrm{He}(\gamma_V, K^+)^3_\Lambda\mathrm{H}$. (a) Impulse approximation; the shaded region corresponds to a pair of nucleon-spectators. (b) KN interaction in the final state. Note that momentum integration of $\vec{p}_z = (0, 0, p_z)$ can no longer be easily removed by renormalizing $\Psi^{^3\mathrm{He}}_{lsL_i}$.

which vanish when $\vec{k}\vec{\epsilon} = 0$. Regarding Born terms, gauge invariance broken by form factor inclusion is restored by contact term implementation (see formula (B1) of [18]). This single channel formalism used in the present calculations also includes energy-dependent widths of the hadron resonances that can be considered to be a partial restoration of unitarity of photo- and electroproduction amplitude.

The parameters of the hadron resonances of the model [17] for neutron processes (2) were selected in such a way that with a constant amount of sum $K^{[\bar{s}][\bar{t}=0]}$ and $K^{[\bar{s}][\bar{t}=1]}$ their difference allowed one to describe the data from [1] quite well. The changes carried out in this way in the model [17] affected only the isoscalar k_s and isovector k_v constants of the resonance coupling: $P_{11}(1440)$ $(k_s^M = 0.18, k_v^M = 0.252)$, $S_{11}(1535)$ $(k_s^E = -0.16, k_v^E = -0.2)$, $S_{11}(1650)$ $(k_s^E = 0.1, k_v^E = -0.214)$, $F_{15}(1860)$ $(k_s^M = 0.8, k_v^M = 0.87, k_s^E = 0.15, k_v^E = 0.18)$, $P_{11}(1880)$ $(k_s^M = -0.003, k_v^M = -0.11)$, $D_{13}(1875)$ $(k_s^E = 0, k_v^E = 0.01)$, $P_{13}(1920)$ $(k_s^M = -0.07, k_v^M = -0.091)$, and $F_{17}(1990)$ $(k_s^M = 0.25, k_v^M = 0.36)$. As total decay width of hadron resonances also includes terms without kaons, the calculations of resonance widths have been extended to other channels. The parameters of the hadron resonances in kaon free channels were assumed to be equal to the parameters of the resonances of the previous work [19], in which a model of double neutral pseudoscalar meson $(\pi^0\pi^0, \pi^0\eta)$ photoproduction on light nuclei was constructed. Such hadron coupling constants transfer ensures the systematicity of the calculations being made.

The pointlike character of the interaction of a high-energy photon with the nucleus and high momentum transfer to the active nucleons ensure the applicability of the impulse approximation, according to which the nuclear amplitude

$$\langle B, K|\hat{t}_{1\mathrm{A}}(Q^2, W_N, \vec{k}, \vec{q}, \vec{p}_{1f})|A, \gamma\rangle = \langle B, K|\sum_{i=1}^{A}\hat{t}_i(Q^2, W_N, \vec{k}, \vec{q})|A, \gamma\rangle \quad (6)$$

is equal to the coherent sum of the single-nucleon operators sandwiched by nuclear wave functions. In (6), the wave function $\langle B|$ is equal to the eigenstate of the final hypernucleus in the coherent processes and the sum of hyperon and the residual nuclear system wave functions in incoherent processes. The index i in (6) denotes an active nucleon whose momentum after the kaon emission is equal to $\vec{p}_{1f}$. In the impulse approximation, the wave functions of kaons and of quasifree hyperons, as for a photon, are treated as plane waves. The model [20] for the deuteron and the projection of the exact three-body wave function $\Psi(\vec{p}, \vec{s})$ [21] for ^{3}He in partial wave channels $^1S_0$-S, $^3S_1$-S, $^3S_1$-D, $^3D_1$-S, and $^3D_1$-D were used as the initial wave functions $|A\rangle$. For a coherent process $^3\mathrm{He}(\gamma_V, K^+)^3_\Lambda\mathrm{H}$, the momentum $\vec{p}_{1f}$ becomes a function of the integration variable: the relative momentum $\vec{p}$ of the active nucleon and the spectator pair (see Fig. 1),

$$\vec{p}_{1f} = \vec{p} - \vec{q} + \frac{A-1}{A}\vec{k}, \qquad \vec{p}' = \frac{A-1}{A}(\vec{k} - \vec{q}) + \vec{p}. \quad (7)$$

Here atomic mass $A = 3$ for the ^{3}He nucleus. The difference between masses of final nucleons and hyperon in (7) is not significant and they are assumed to be identical there. The calculation of the matrix element (6) sandwiched by the nuclear wave functions is performed in the LSJ (where L-orbital, S-spin, J-total angular moment of the system) representation. In this coupling scheme, each term of the right part (6) for the incoherent process $^3\mathrm{He}(\gamma_V, K^+\Lambda)X$ has the form

$$\langle \Lambda + X, K^+|\hat{t}_i(Q^2, W_N, \vec{k}, \vec{q})|^3\mathrm{He}, \gamma\rangle = \sum_{JM_J s l L_i}\sum_{m_l m_s M_{S_i}\bar{m}_s} C^{S_i M_{S_i}}_{sm_s\, SM_{S_i}-m_s} C^{JM_J}_{L_i M_J - M_{S_i}\, S_i M_{S_i}} C^{L_i M_J - M_{S_i}}_{lm_l\, LM_J - M_{S_i} - m_l} (-1)^{\bar{m}_s} \hat{t}^{\bar{s}} C^{s' m_{s'}}_{sm_s\, \bar{s}-\bar{m}_s} (K^{[\bar{s}][\bar{t}]})_{\bar{m}_s} \frac{\Psi^{^3\mathrm{He}}_{lsL_i}(p,s) Y_{lm_l}(\hat{p}) Y_{L_i M_J - M_{S_i} - m_l}(\hat{s})}{\sqrt{\sum_\nu \int \left(\Psi^{^3\mathrm{He}}_{lsL_i}(p,s)\right)^2 d^3p}}. \quad (8)$$

Here $\Psi^{^3\mathrm{He}}_{lsL_i}(p,s)$ are the components of the helium-3 wave function, depending on the modules of the relative momentum of the active nucleon (p) in the CMS and the relative momentum of the pair of nucleon spectators (s) [see Fig. 1(a)]. Spherical harmonics $Y_{lm_l}(\hat{p})$ and $Y_{L_iM_J-M_{S_i}-m_l}(\hat{s})$ depend on the angular variables associated with the momenta $\vec{p}$ and $\vec{s}$.

For coherent processes, the nuclear matrix element is equal to

$$\begin{aligned}
&\left\langle {}^3_\Lambda\mathrm{H}, K^+\middle|\hat{t}_i(Q^2, W_N, \vec{k}, \vec{q})\right|{}^3\mathrm{He}, \gamma\rangle \\
&= \sum_{JM_JslL_i}\sum_{m_lm_sM_{S_i}\bar{m}_s} C^{S_iM_{S_i}}_{sm_s\,SM_{S_i}-m_s} C^{JM_J}_{L_iM_J-M_{S_i}\,S_iM_{S_i}} C^{L_iM_J-M_{S_i}}_{lm_l\,LM_J-M_{S_i}-m_l} (-1)^{\bar{m}_s} i^{\bar{s}} C^{s'm_{s'}}_{sm_s\,\bar{s}-\bar{m}_s} \sum_{s'l'L_f}\sum_{m_{l'}m_{s'}M_{S_f}} C^{S_fM_{S_f}}_{s'm_{s'}\,SM_{S_f}-m_{s'}} \\
&\times C^{JM_J}_{L_fM_J-M_{S_f}\,S_fM_{S_f}} C^{L_fM_J-M_{S_f}}_{l'm_{l'}\,LM_J-M_{S_f}-m_{l'}} \int \frac{d^3p\,d^3s}{(2\pi)^3} \Psi^{^3_\Lambda\mathrm{H}}_{l's'L_f}(p',s) Y^*_{l'm_{l'}}(\hat{p}') Y^*_{L_fM_J-M_{S_f}-m_{l'}}(\hat{s}) \\
&\times (K^{[\bar{s}][\bar{t}]})_{\bar{m}_s} \Psi^{^3\mathrm{He}}_{lsL_i}(p,s) Y_{lm_l}(\hat{p}) Y_{L_iM_J-M_{S_i}-m_l}(\hat{s}).
\end{aligned} \tag{9}$$

The isotopic structure of the nuclear matrix elements (8) and (9) is identical and has the form

$$(-1)^{T+T_i+t'+\bar{t}}\sqrt{2T_i+1}\sqrt{2t'+1}C^{T_fM_f}_{T_iM_i\,\bar{t}-\bar{m}}\begin{pmatrix} t & T & T_i \\ T_f & \bar{t} & t' \end{pmatrix}. \tag{10}$$

The notation used in (10) for the $6j$ symbol is t, t': isospins of the initial nucleon and the final hyperon; T_i, T_f: full initial and final isospins; T: isospins of a pair of nucleon spectators; $\bar{t}$, $\bar{m}$: the transferred isospin and its projection. For a coherent process, $T_f = 0$ since the hypertriton isospin is zero.

For an incoherent process $^3\mathrm{He}(\gamma_V, K^+\Lambda)X$, isospin $T_f = 0$ when X is a bound proton-neutron pair, and $T_f = 1$ when X is a proton pair (channels $K^0\Lambda$, $K^0\Sigma^0$, $K^+\Sigma^-$). Isotopic structure (10) for coherent and incoherent processes of kaon photo- and electproduction on ^{3}He for all channels (1) and (2) is reduced to a multiplier of $1/\sqrt{2}$ from the formula (10).

The unpolarized cross section of the kaon electroproduction is

$$\frac{d\sigma(Q^2)}{d\Omega^{cm}_K} = \frac{d\sigma_T(Q^2)}{d\Omega^{cm}_K} + \varepsilon\frac{d\sigma_L(Q^2)}{d\Omega^{cm}_K}, \tag{11}$$

where Ω^{cm}_K is the solid angle characterizing the kaon emission in the CMS. In (11) σ_T and σ_L are the cross sections associated with the transverse and longitudinal components of the photon polarization vector $\vec{\epsilon}_\lambda$. The photon polarization index takes the values $\lambda = -1, 0, +1$. The polarization degree of the photon beam is $\varepsilon \in [0, \ldots, 1]$. For the experiments [4,5] one has $\varepsilon = 0.765$.

For coherent processes, the right part of the formula (11) takes the form

$$\frac{d\sigma(Q^2)}{d\Omega^{cm}_K} = (2\pi)^{-2}\frac{E_i\sqrt{\omega^2_K - M^2_K}E_f}{4\omega_\gamma W^2}\frac{1}{2(2J+1)}(|T_{\lambda=\pm1}|^2 + 2\varepsilon|T_{\lambda=0}|^2). \tag{12}$$

The energies of the initial and final nuclei in (12) are denoted as E_i, E_f, respectively. The energy and the mass of the kaon are ω_K and M_k, respectively. For the nuclear transition amplitudes in (12) for photons of longitudinal and transverse polarization quantities $T_{\lambda=0}$ and $T_{\lambda=\pm1}$ are introduced.

For an incoherent process $^3\mathrm{He}(\gamma_V, K^+\Lambda)X$, the cross section of the kaon electroproduction has the form

$$\frac{d\sigma(Q^2)}{d\Omega^{cm}_K d\Omega_{YX} d\omega_{YX}} = (2\pi)^{-5}\frac{E_i p_{YX}\sqrt{\omega^2_K - M^2_K}M_X M_Y}{4\omega_\gamma W^2}\frac{1}{2(2J+1)}(|T_{\lambda=\pm1}|^2 + 2\varepsilon|T_{\lambda=0}|^2), \tag{13}$$

in which p_{YX} is the relative momentum in the subsystem YX with the masses of nuclides M_Y and M_X. Ω_{YX} is the solid angle at which the nuclides Y and X are visible in their own center-of-mass system with invariant mass ω_{YX}.

III. WAVE FUNCTIONS OF THREE-BODY SYSTEMS

In this work, along with the use of the parametrization from [21] for the wave function ^{3}He, the eigenfunctions of the nuclei ^{3}He and $^3_\Lambda$H are obtained by solving the homogeneous Faddeev equation at the point E_B, the binding energy of a three-body system. The algebraic approximation of the homogeneous Faddeev equation on an $N \times N$ grid of momenta p and s written for three bodies of different masses has the form

$$\left[\begin{pmatrix} 1_{N\times N} & 0 & 0 \\ 0 & 1_{N\times N} & 0 \\ 0 & 0 & 1_{N\times N} \end{pmatrix} - \begin{pmatrix} 0 & a_{12} & a_{13} \\ a_{21} & 0 & a_{23} \\ a_{31}0 & a_{23} & 0 \end{pmatrix}\right]_{E_B}\begin{pmatrix} \Psi_{1\times(1-N)} \\ \Psi_{1\times(N+1-2N)} \\ \Psi_{1\times(2N+1-3N)} \end{pmatrix} = \begin{pmatrix} 0 \\ 0 \\ 0 \end{pmatrix}. \tag{14}$$

Components of a numeric vector ($\Psi_{1\times(1-N)}$, $\Psi_{1\times(N+1-2N)}$, $\Psi_{1\times(2N+1-3N)}$) [22] give an expression for the total three-body wave function Ψ in the particle representation:

$$\begin{aligned}\Psi_{(31)2} &= \Psi_{1\times(1-N)} - \Psi_{1\times(N+1-2N)} + \Psi_{1\times(N+1-2N)},\\ \Psi_{(12)3} &= \Psi_{1\times(1-N)} + \Psi_{1\times(N+1-2N)} - \Psi_{1\times(N+1-2N)},\\ \Psi_{(23)1} &= -\Psi_{1\times(1-N)} + \Psi_{1\times(N+1-2N)} + \Psi_{1\times(N+1-2N)}.\end{aligned} \tag{15}$$

Here 1,2,3 are the particle numbers of the nuclei ^{3}He and $^3_\Lambda$H. Each of the components of Ψ is normalized to unity,

$$\sum_\nu \int d^3s\, d^3p\, \Psi_\nu^2(p,s) = 1. \tag{16}$$

Summation in (16) is carried out over partial-wave channels in which the complete function has expansion coefficients $\Psi_\nu(p,s) \equiv \Psi_{lsL}(p,s)$. The components $a_{i>j}, a_{j>i}$, $i,j = 1,2,3$ take the form

$$\begin{aligned}a_{12} &= \left(E_B - \frac{s^2}{2\mu_{23}} - \frac{p^2}{2M_{2(31)}}\right)^{-1} \int d^3q'' t_1\left(q'', s, \cos(\theta_{sq''}), E_B - \frac{p^2}{2M_{2(31)}}\right),\\ a_{13} &= \left(E_B - \frac{s^2}{2\mu_{23}} - \frac{p^2}{2M_{3(12)}}\right)^{-1} \int d^3q'' t_1\left(q'', s, \cos(\theta_{sq''}), E_B - \frac{p^2}{2M_{3(12)}}\right),\\ a_{21} &= \left(E_B - \frac{s^2}{2\mu_{31}} - \frac{p^2}{2M_{1(23)}}\right)^{-1} \int d^3q'' t_2\left(q'', s, \cos(\theta_{sq''}), E_B - \frac{p^2}{2M_{1(23)}}\right),\\ a_{23} &= \left(E_B - \frac{s^2}{2\mu_{31}} - \frac{p^2}{2M_{3(12)}}\right)^{-1} \int d^3q'' t_2\left(q'', s, \cos(\theta_{sq''}), E_B - \frac{p^2}{2M_{3(12)}}\right),\\ a_{31} &= \left(E_B - \frac{s^2}{2\mu_{12}} - \frac{p^2}{2M_{1(23)}}\right)^{-1} \int d^3q'' t_3\left(q'', s, \cos(\theta_{sq''}), E_B - \frac{p^2}{2M_{1(23)}}\right),\\ a_{32} &= \left(E_B - \frac{s^2}{2\mu_{12}} - \frac{p^2}{2M_{2(31)}}\right)^{-1} \int d^3q'' t_3\left(q'', s, \cos(\theta_{sq''}), E_B - \frac{p^2}{2M_{2(31)}}\right).\end{aligned} \tag{17}$$

$M_{i(jk)}$ is the reduced mass of the active particle i relative to a pair of spectator jk nucleons. Two-body t matrices in (17) are determined by the interaction in a pair of particles $t_1 \to (23)$, $t_2 \to (31)$, $t_3 \to (12)$. Integration in (16) is carried out by the relative momentum in the interacting pair of particles. Taking into account nontrivial kinematic connections in the selected coordinate system [22,23] polar angle $\cos(\theta_{sq''})$ of the on-shell momentum s becomes a function of the solid angle of $\vec{q}''$ and the modules q'' and s.

The Bonn [24] model for NN potential and the models [25,26] for YN interactions were used as two-body input generating t matrices. The phenomenological model [25] based on the coupled Lippmann-Schwinger equations allows one to describe fairly well the few experimental data on YN interaction in the low energy region and accurately takes into account the conversion of $\Sigma N \to \Lambda N$. The microscopic extended soft-core (ESC) model of ΛN [26] was reproduced using a computer code available at [26], which allows one to calculate the coordinate components of YN potentials in given partial wave states. Then, these components of coordinate potentials using Fourier transforms [27] were used solving a coupled Lippmann-Schwinger equations to obtain two-body t matrices.

Figure 2 shows the component Ψ_{NNN} in the partial wave $^1S_0$-S of the total wave function of the ^{3}He nucleus obtained from the system (14). For comparison, the parametrization of [21] for the same partial wave is also shown there. Figure 2 also shows calculations of the $\Psi_{NN\Lambda}$ function in the $^1S_0$-S wave using phenomenological YN [25] and microscopic [26] models. Subsequently, these wave functions are used to calculate the cross sections of processes $^3\mathrm{He}(\gamma_V, K^+)^3_\Lambda\mathrm{H}$ and $^3\mathrm{He}(\gamma_V, K^+\Lambda)X$.

IV. FINAL STATE INTERACTION

Taking into account the interaction in the final state, the nuclear amplitude T_λ should contain the additional contributions to the impulse approximation (8)

$$\begin{aligned}T_\lambda &= t_{\mathrm{IA}}(Q^2, W_N, \vec{k}, \vec{q}, \vec{p}_{1f}) + t_{\mathrm{FSI}}(Q^2, W_N, \vec{k}, \vec{q}, \vec{p}_{1f}),\\ t_{\mathrm{FSI}}(Q^2, W_N, \vec{k}, \vec{q}, \vec{p}_{1f}) &= \int \frac{d^3p'}{(2\pi)^3} \frac{(t_{KN} + t_{KY} + t_{NY})}{\omega(p') - \omega(p) + i\epsilon} t_{\mathrm{IA}}(Q^2, W_N, \vec{k}, \vec{q}, \vec{p}_{1f}).\end{aligned} \tag{18}$$

The two-body t matrices in (18) depend only on the relative momenta of the KN, KY, and NY subsystems before and after the interaction. For simplicity, in (18), arguments for t matrices and summation over projections of intermediate spins of the interacting particle subsystem are omitted. The imaginary term $i\epsilon$ in the denominator (18) provides a correct bypass of the pole that occurs at the point $p' = p$, at which the

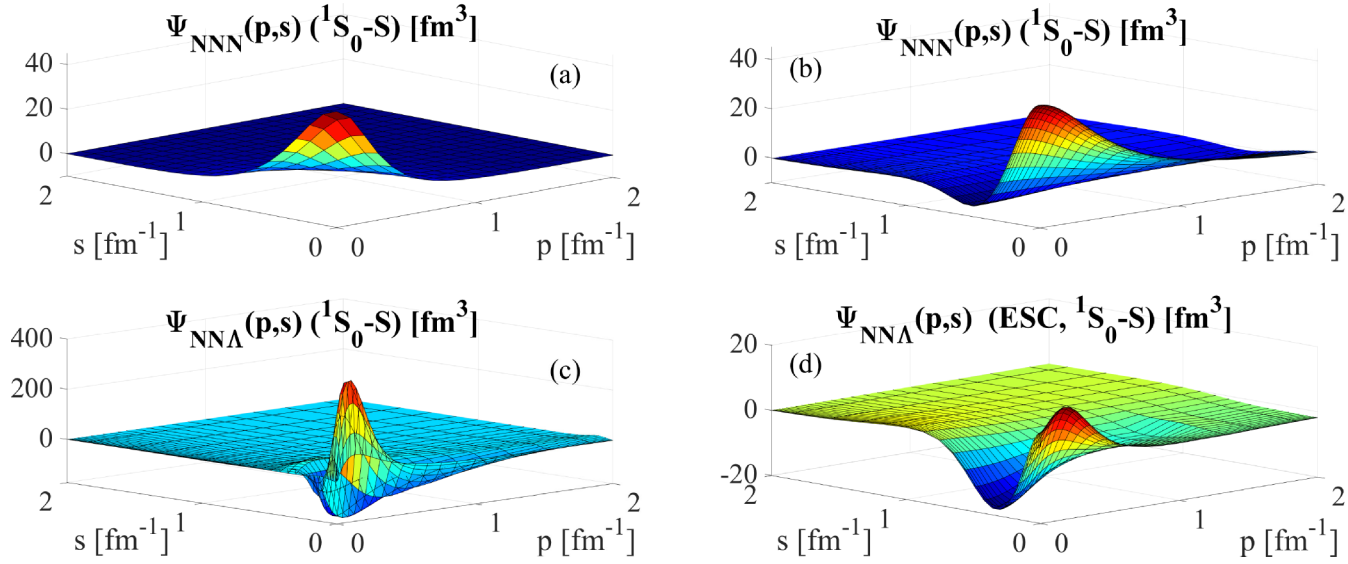

FIG. 2. (a),(b) Components of the full wave function ^{3}He in the partial wave $^1S_0$-S in the parametrization of the work [21] and in the calculations of this work, respectively. (c),(d) Components of the full wave function $^3_\Lambda$H in the partial wave $^1S_0$-S, obtained using phenomenological [25] and microscopic [26] YN models, respectively.

energy $\omega(p')$ of a kaon or hyperon in the loop coincides with the energy of the same particle $\omega(p)$ on the mass shell. In the pole approximation, the momentum of a final hyperon $\vec{p}_{1f}$ is

$$\vec{p}_{1f} = -\frac{M_K + M_N}{M_K}\vec{q} + \vec{p}'\frac{M_K + M_N}{M_N}. \tag{19}$$

For a coherent process $^3\mathrm{He}(\gamma_V, K^+)^3_\Lambda\mathrm{H}$, the interaction in the final state in the pole approximation is also reduced to equality of relative momenta (kaon, hyperon) before and after the interaction. Finally for a coherent process on ^{3}He, the momentum of the active particle in the final state is

$$\vec{p}_{1f} = -\vec{p}' + \frac{\vec{p}_z + \vec{k}}{2}. \tag{20}$$

As one can see, the presence of the second loop [see Fig. 1(b)] in a coherent process leads to a more complex dependence of the momentum of the active nucleon on the integration variables. Note that the choice of the z axis can be provided by $\vec{s} = \vec{p}_z$.

Figure 3 shows the processes of final state interaction, which are taken into account in this work. The contribution of the two-step process $\gamma_V N \to \pi N \to KY$, which involves the spectator nucleons of the target nucleus, is neglected in this work. The reason for this is that the structure of the elementary process $\pi N \to KY$ is not well studied yet. Note the work [28], which gives estimations of the differential cross section $d\sigma/d\Omega$ of the process $\pi^+ n \to K^+\Lambda$ depending on the incident-pion momentum in the laboratory frame.

The following models of two-body interactions were used: the dynamical coupled-channel (DCC) KN model [29] in the s-wave approximation, the chirally motivated (ChM) KN model [30], the microscopical KY model [31] for $K\Lambda$ and $K\Sigma$ interactions, and the hyperon-nucleon phenomenological (Ph.) [25] and microscopical (ESC) [26] models. Here one can briefly analyze the magnitude of the considered effects of interaction in the final state on the reaction $^2\mathrm{H}(\gamma, K^0\Lambda)^1\mathrm{H}$ for example. Figure 4 shows the ratio of total cross sections calculated with and without YN and KN interactions in the final state at two energies. As a variable on the abscissa axis, the relative impulses $p_{YN/KN}$ in the subsystems YN and KN are given, which are related to the invariant mass $\omega_{YN/KN}$ of the corresponding

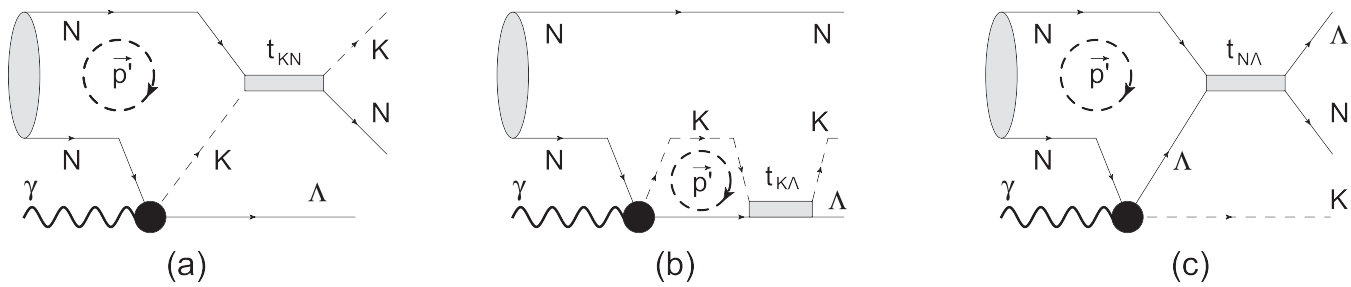

FIG. 3. Final state interaction in a two-nucleon system: (a) KN, (b) $K\Lambda$, (c) $N\Lambda$. A dashed circle with an arrow indicates integration over a loop momentum. Filled circles correspond to the elementary operator of kaon photo- and electroproduction.

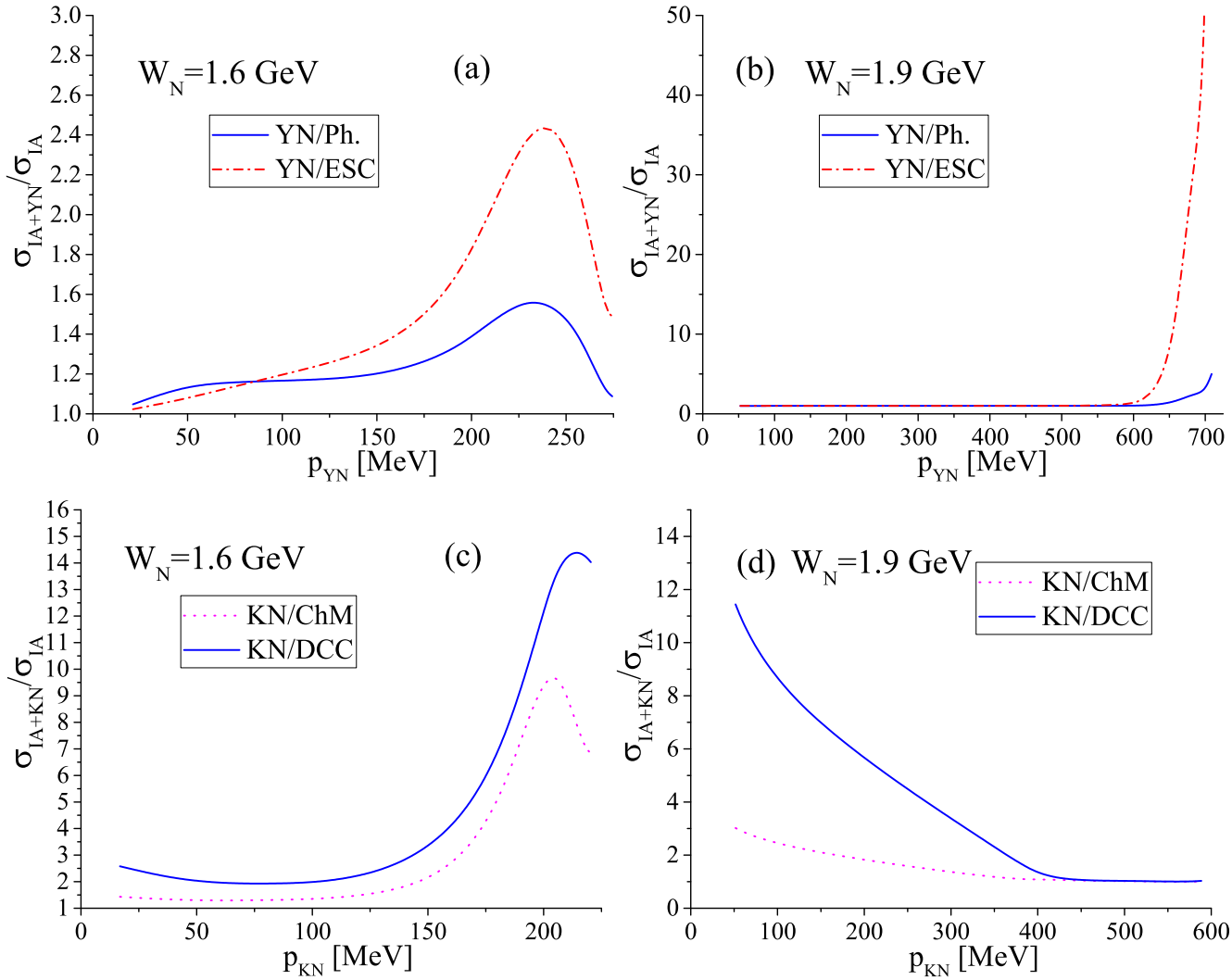

FIG. 4. The relative contributions of YN (a), (b) and KN (c), (d) final state interactions to the total cross section of the reaction $^2\mathrm{H}(\gamma, K^0\Lambda)\,^1\mathrm{H}$ at two energies $W_N = 1.6$, 1.9 GeV. Hyperon-nucleon (kaon-nucleon) interactions are calculated in the top (bottom) panel with the use of Ph. [25] and ESC [26] models (ChM [30] and DCC [29] models).

subsystems by the formula

$$p_{YN/KN} = \frac{\sqrt{\left(\omega^2_{YN/KN} - (M_{Y/K} - M_N)^2\right)\left(\omega^2_{YN/KN} - (M_{Y/K} + M_N)^2\right)}}{2\omega_{YN/KN}}. \tag{21}$$

I also introduced masses of hyperon (M_Y), kaon (M_K), and nucleon (M_N) in (21). In the near-threshold region at $W_N =$ 1.6 GeV, the contributions of YN and KN interactions are maximal for relative momenta $p_{YN} = 200$–250 MeV and $p_{KN} = 150$–230 MeV, respectively. The maximum relative contribution of YN final interaction was 1.4–2.4 times, while the relative contribution of KN final state interaction reaches 9–15 times in corresponding momentum regions. The large final state interaction effect in the near-threshold region is not surprising by itself and was noted, for example, in [32] for the reaction $d(\gamma, \eta)np$. It is noteworthy that in the processes $^2\mathrm{H}(\gamma, \eta)n^1\mathrm{H}$, and $^2\mathrm{H}(\gamma, K^0\Lambda)\,^1\mathrm{H}$, the influence of ηN and KN interactions in the final state is maximal in the region of large invariant masses of the corresponding subsystems. With an increase in the energy of W_N, the behaviors of YN and KN interactions differ. At $W_N = 1.9$ GeV, the interaction of YN remains noticeable only in the region of large relative momenta of p_{YN}, while KN still makes the main contribution in the region of small p_{KN}. The existence of local maxima in YN and KN interactions in the momentum range of 200–250 MeV can be related to the dynamic features of the models of KN and YN interactions used. The difference between the predictions of final YN or KN interactions of models used can be up to several times at defined relative momenta. In the next section, it will be shown that despite the variation in the magnitude of the interaction effect in the final state, the

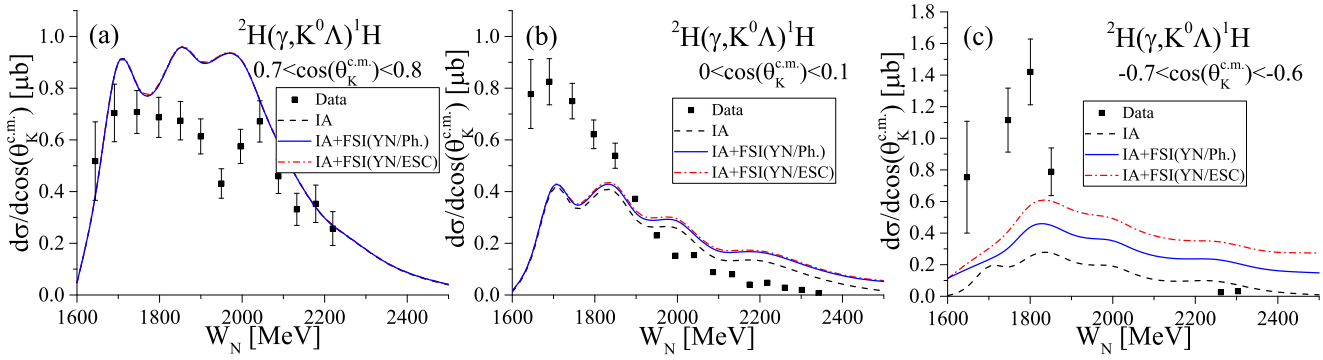

FIG. 5. Differential cross sections of $^2\mathrm{H}(\gamma, K^0\Lambda)^1\mathrm{H}$ in three different areas of the kaon emission angles in the center of mass (c.m.) frame: $\cos(\theta_K^{\mathrm{c.m.}}) = 0.75$ (a), 0.05 (b), −0.65 (c). Contributions of final state interactions (see Fig. 3) have been marked with solid blue lines (with the phenomenological YN [25] model) and with red dash-dotted lines (with the ESC [26] YN model). Data are from [1].

available experimental data are not enough to unambiguously filter out certain models.

V. RESULTS AND DISCUSSION

The results of calculations of total and differential cross sections of the processes considered in this work are shown in Figs. 5–9. First, the differential cross sections of quasi-free kaon photoproduction on a neutron in the reaction $^2\mathrm{H}(\gamma, K^0\Lambda)^1\mathrm{H}$ were calculated (see Fig. 5). Experimental data [1] on this process allow one to calibrate the model of kaon photoproduction in a sufficiently wide range of kaon emission angles and in a wide range of photon energies. The results of such simple calibration of the model from [17] according to data [1] for the values of the kaon emission angles $\cos(\theta_K^{\mathrm{c.m.}}) = 0.75, 0.05, -0.65$ are shown in Fig. 5. It can be seen that, in the area of $\cos(\theta_K^{\mathrm{c.m.}}) = 0.75$, the present model conveys the features of the cross section well. The contribution of the considered final state interaction in the region of small kaon emission angles turns out to be negligible. In the regions $\cos(\theta_K^{\mathrm{c.m.}}) = 0.05, -0.65$, the contributions of the final state interaction, in contrast, become more noticeable. One can expect that with $W_N \approx 1.8$ GeV and at $\cos(\theta_K^{\mathrm{c.m.}}) \approx -0.65$ the contributions of the impulse approximation and the final state interaction are comparable. Apparently, the too high contribution of the processes of Fig. 3 in the area of $\cos(\theta_K^{\mathrm{c.m.}}) = -0.65$ is due to the absence in the formula (18) of additional form factors suppressing the KN, $K\Lambda$, and ΛN interactions at high momentum transfer. The influence of such additional damping factors in the formula (18) will remain the subject of further research. Note that the resonant kaon emission of the model from [17] on a neutron in the region of large angles may be slightly increased in the future for a better agreement with the data of [1].

At the next stage, the differential cross sections of the kaon electroproduction on the deuteron in three different charge channels, $K^+\Lambda$, $K^+\Sigma^0$, and $K^+\Sigma^-$, were calculated at $W_N = 1.91$ GeV, $Q^2 = 0.35$ GeV^2 (see Fig. 6). From the comparison of these calculations with the experiment in [5], it follows that the predictions of the present model are in quite good agreement with data. The contribution of the final state interaction processes turns out to be significant for the $K^+\Sigma^0$ channel, in which K^+n, $K^+\Sigma^0$, $\Sigma^0 n$ interactions take place. The leading role in these processes is played by the $\Sigma^0 n$ interaction,

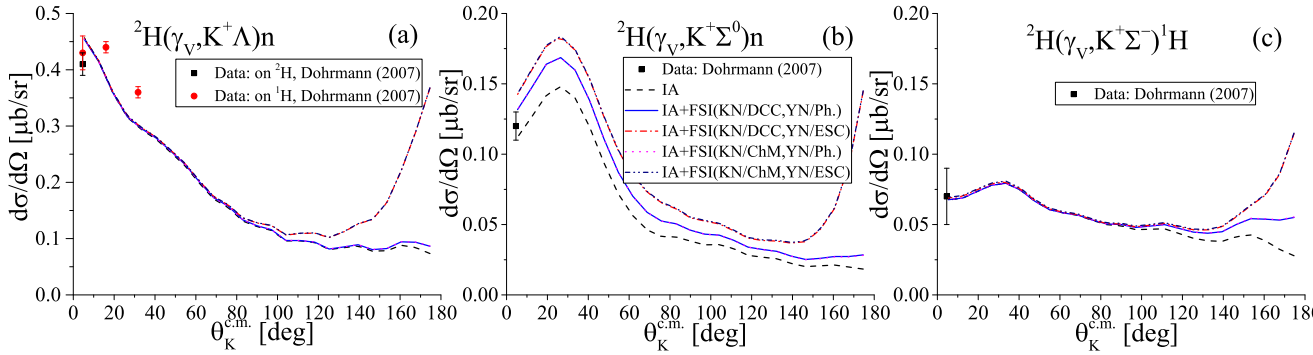

FIG. 6. The differential cross section of the kaon electroproduction on a deuteron at $W_N = 1.91$ GeV, $Q^2 = 0.35$ GeV^2 in three different charge channels: $K^+\Lambda$ (a), $K^+\Sigma^0$ (b), $K^+\Sigma^-$ (c). The contributions of the final state interaction processes (see Fig. 3) are shown by solid blue lines (KN DCC model [29] with phenomenological YN model [25]), dash-dotted red lines (KN DCC model [29] with microscopical YN model [26]), dotted magenta lines (chirally motivated KN model with phenomenological YN model [25]), and navy dash-two-dotted lines (chirally motivated KN model with microscopical YN model [25]). For the KY interactions the microscopical model [31] was used. Data are from [5].

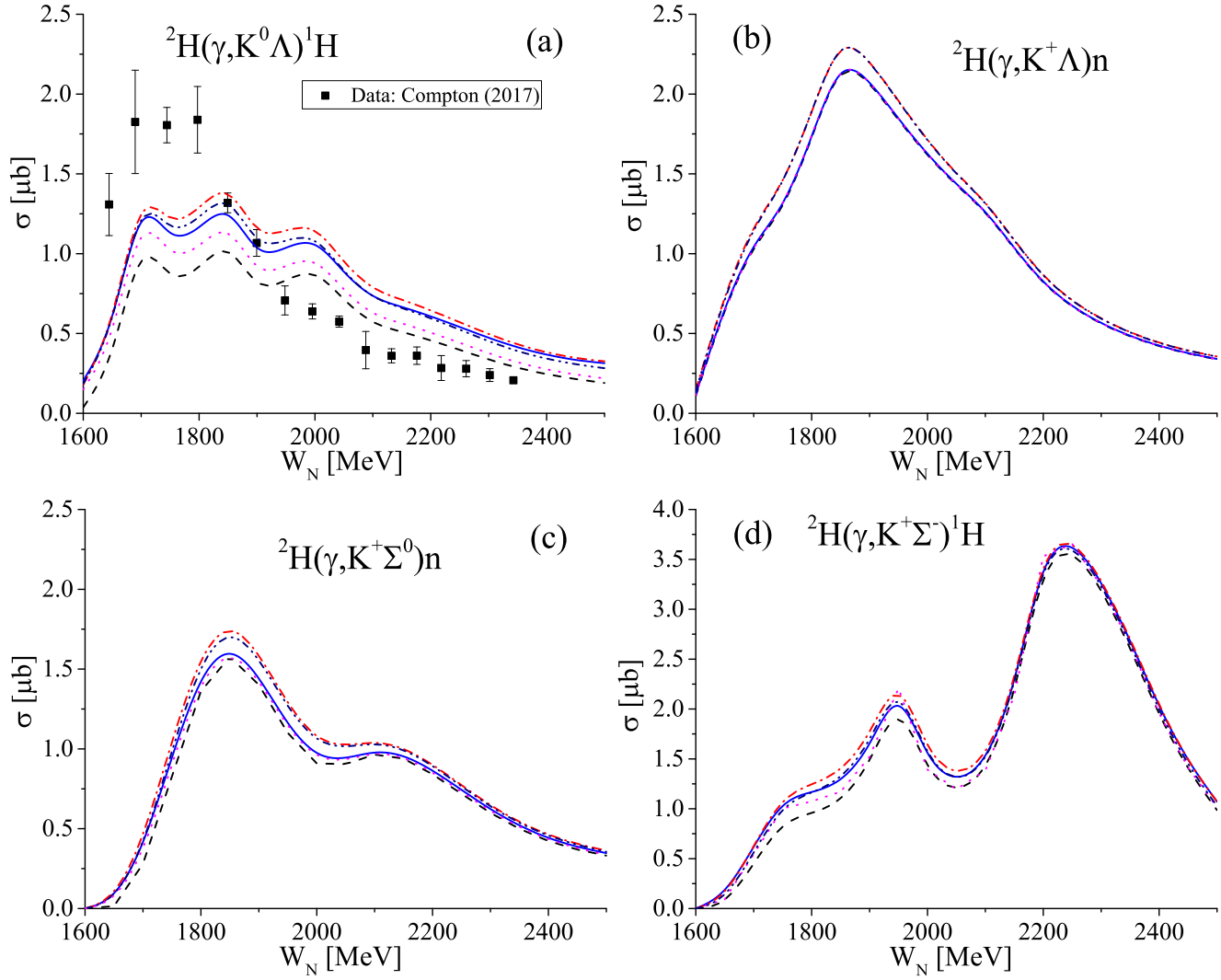

FIG. 7. Total cross sections of the kaon photoproduction in the four possible charge channels: $K^0\Lambda$ (a), $K^+\Lambda$ (b), $K^+\Sigma^0$ (c), $K^+\Sigma^-$ (d). Calculations without and with the final state interaction processes (see Fig. 3) are shown. The designation of the lines is the same as in Fig. 6. Data are from [1].

calculated in this work using the phenomenological model [25]. For the $K^+\Sigma^-$ channel, the impulse approximation seems to be in fairly good agreement with the experiment in the region of $\cos(\theta_K^{\text{c.m.}}) \approx 0$. Note that the production of $K^+\Sigma^-$ occurs on a neutron, for which the present model was previously calibrated according to experimental data [1], and the isotopic contributions of $T = 1/2$ resonances in the channel $K^+\Sigma^-$ are $\sqrt{2/3}$ times less than in the channel $K^0\Lambda$ for which a reasonable agreement with the experiment (see Fig. 5) was obtained in the region $\cos(\theta_K^{\text{c.m.}}) = 0.75$. Final state interactions of K^+p and Σ^-p seem to be partially compensated by each other in the $K^+\Sigma^-$ channel. Final state K^+n interaction in the $K^+\Sigma^0$ channel is less than K^+p interaction in the $K^+\Sigma^-$ channel, which results in a more sizable final state interaction effect in the $K^+\Sigma^0$ channel due to uncompensated $\Sigma^0 n$.

Figure 7 shows the results of calculations of the total cross sections of kaon photoproduction on a deuteron in four possible charge channels. Comparison with the experiment [1] for the $K^0\Lambda$ channel indicates the need to introduce an additional damping factor into the formula (18), which would ensure suppression of the excessive final state interaction processes' growth in the region $W_N > 1.9$ GeV. As before, for the $K^+\Lambda$ channel, the contribution of final state interaction processes is noticeably less than for the $K^0\Lambda$ channel, which is associated with a weaker K^+n interaction compared to $K^{0,+}p$. For the same reasons, the final state interaction contributions in the channels $K^+\Sigma^0$ and $K^+\Sigma^-$ differ. Unfortunately, there are no experimental total cross sections for the last two channels, nor for the $K^+\Lambda$ channel, for a more representative comparison with theory.

A more complicated situation is observed in the calculations of the cross sections of kaon photo- and electroproduction on ^{3}He. In this case, not does only the number of possible interaction processes in the final state increase, but also the peculiarities of calculations of the target nucleus wave functions—as well as the final nucleus wave function, in the case of coherent processes–manifest themselves. Figure 8 (left) shows the differential cross section of the kaon

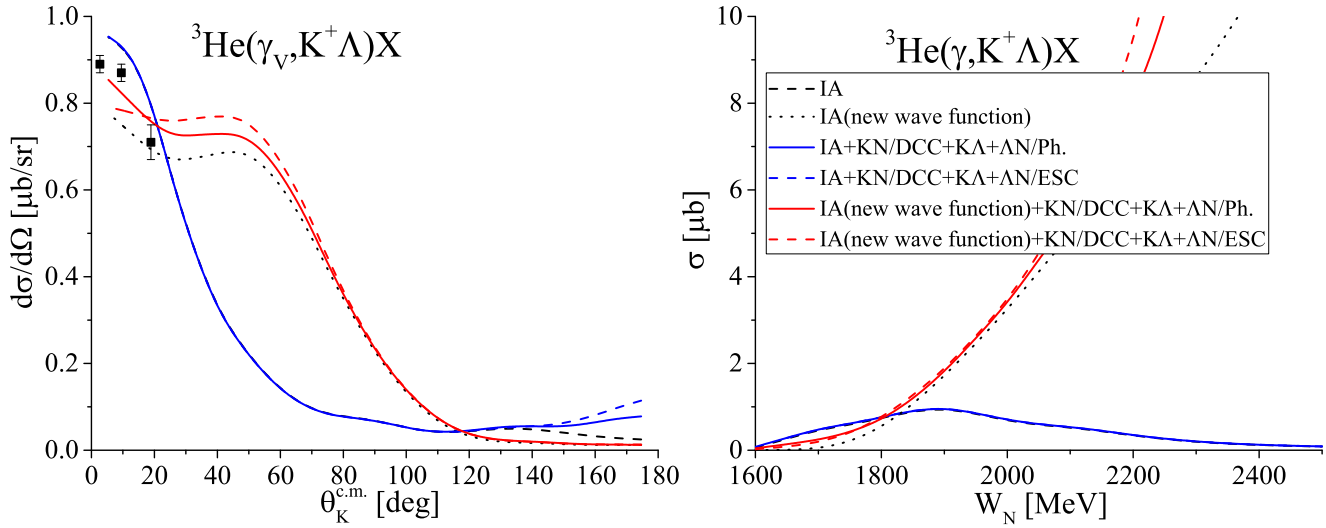

FIG. 8. Left: the differential cross section of the kaon electroproduction in incoherent process ^{3}He(γ_V, $K^+\Lambda$)X at $W_N = 1.91$ GeV, $Q^2 = 0.35$ GeV^2. In calculations the target eigenfunction of [21] and the function obtained in this work (new wave function) were used. The models of interaction in the final state are described in the text. Data are from [5]. Right: the total cross section of the incoherent process ^{3}He(γ_V, $K^+\Lambda$)X, obtained with and without taking into account the final state interaction (see Fig. 3) with different eigenfunctions of the target nucleus.

electroproduction in the incoherent process ^{3}He(γ_V, $K^+\Lambda$)X at $W_N = 1.91$ GeV, $Q^2 = 0.35$ GeV^2, obtained with and without taking into account the final state interaction, as well as using the helium-3 wave function of [21] and the function obtained in this work by solving Eq. (14). Additionally, the different ΛN interaction models [25,26] were used. These models are not very distinguishable in terms of final state interaction contribution to the cross section. As one can see from Fig. 8 (left), the effect of the final state interaction depends on the type of the target eigenfunction. With the use of the parametrization of [21] for the ^{3}He wave function, the contributions of final state interaction processes are barely noticeable in the region of large kaon emission angles $\theta_K^{c.m.} > 130^\circ$, whereas in the region of small angles their influence is absent, which is consistent with the picture earlier observed for the process ^{2}H(γ, $K^+\Lambda$)n. On the other hand there is a characteristic local maximum in the differential cross section in the region $\theta_K^{c.m.} \approx 50^\circ$ with the eigenfunction obtained in this work. This maximum is absent in calculations with the parametrization from [21]. This behavior of the cross sections is due only to the difference of the wave functions ^{3}He. Indeed, from Figs. 2(a) and 2(b) it can be seen that already for

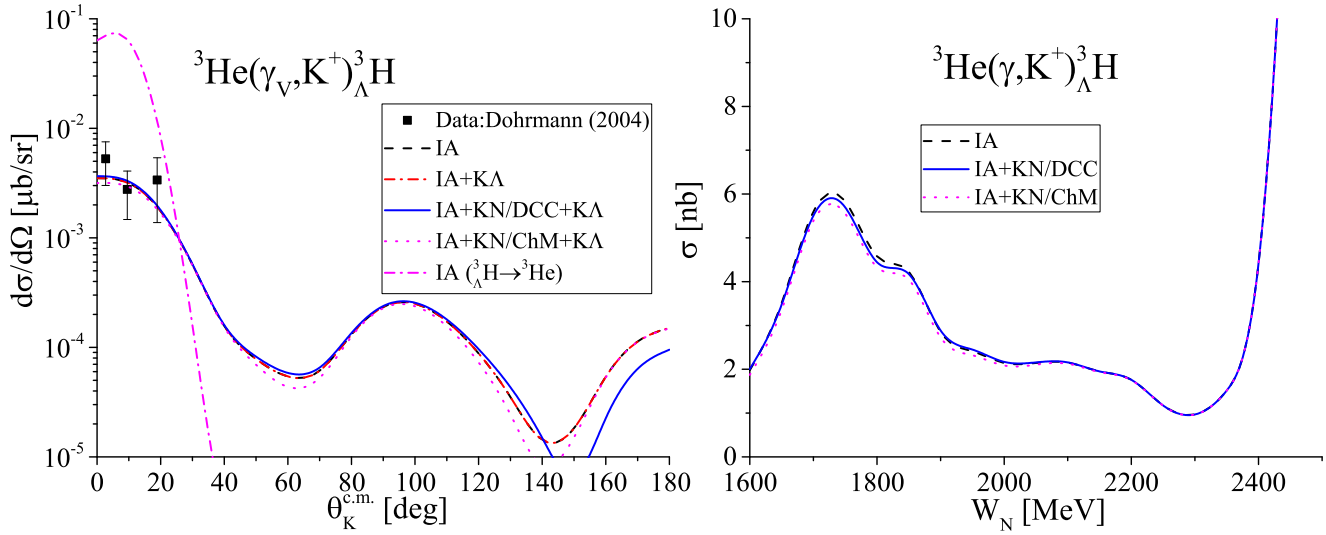

FIG. 9. Left: the differential cross section of the kaon electroproduction ^{3}He(γ_V, K^+)$^3_\Lambda$H at $W_N = 1.91$ GeV, $Q^2 = 0.35$ GeV^2. Additionally, the calculation with the replacement of the hypertriton wave function by the ^{3}He function [21] is presented by the dash-dotted line. The models of final state interaction are described in the text. Data are from [5]. Right: the total cross section of the kaon photoproduction ^{3}He(γ_V, K^+)$^3_\Lambda$H, obtained with and without taking into account the final state interaction (see Fig. 3). The designation of the lines is the same as in Fig. 6.

the leading $^1S_0$-S term the eigenfunction of ^{3}He obtained in this work has a rather more complex structure characterized by a local minimum in the variable s (momentum in a pair of nucleon-spectators) for a wide interval around the variable p (momentum of the active nucleon). The contributions of the final state interaction processes (KN, $K\Lambda$, ΛN) for the ^{3}He wave function obtained in this work are more noticeable already in the region of small kaon emission angles, where the role of the impulse approximation is greater than in calculations with the function from [21]. Note that with the phenomenological model ΛN [25] it is possible to obtain a good agreement of calculations with the data [5], whereas calculations with the function from [21] slightly exceed these data regardless of the interaction processes in the final state. On the right in Fig. 8, the total cross section of the kaon electroproduction in the $^3\mathrm{He}(\gamma_V, K^+\Lambda)X$ process is given, taking into account the final state interactions. As one can see, the leading role in the region of large energy W_N is played by the eigenfunction of the target nucleus. The total cross section $^3\mathrm{He}(\gamma_V, K^+\Lambda)X$ obtained with the function from [21] turns out to be less than the total cross section of the process $^2\mathrm{H}(\gamma, K^+\Lambda)n$ at the same energy W_N. This circumstance corresponds to the previously observed picture of quasi-free pion photoproduction on the deuteron and ^{3}He [15]. Calculations with the function obtained in this work demonstrate a constant growth of the cross section, significantly exceeding calculations with the function from [21] at $W_N > 1.9$ GeV. The contributions of the interaction processes in the final state also correlate with the target function used. The most probable reason for the growth of the cross section $^3\mathrm{He}(\gamma_V, K^+\Lambda)X$ with the function obtained in this work is the nonrelativistic nature of the original equation (14).

Figure 9 (left) shows the differential cross section of coherent kaon electroproduction in the process $^3\mathrm{He}(\gamma_V, K^+)^3_\Lambda\mathrm{H}$ at $W_N = 1.91$ GeV and $Q^2 = 0.35$ GeV^2. The same figure additionally shows the cross section calculations performed with the replacement of the hypertriton wave function by the wave function of the ^{3}He nucleus [21]. It can be seen that in the area of $\theta_K^{\mathrm{c.m.}} < 30^\circ$, the calculation with the replacement of the function of $^3_\Lambda$H by that of ^{3}He within the constant coincides with the exact calculation of the cross section $^3\mathrm{He}(\gamma_V, K^+)^3_\Lambda\mathrm{H}$. A good agreement of the calculations with the experiment confirms the correctness of the found solution of Eq. (14). The effect of the interaction in the final state (KN and $K\Lambda$) turns out to be negligible, noticeable only in the region of large kaon emission angles $\theta_K^{\mathrm{c.m.}} > 140^\circ$. The total cross section of the process $^3\mathrm{He}(\gamma_V, K^+)^3_\Lambda\mathrm{H}$ is shown on the right in Fig. 9. This cross section does not exceed 6 nb in the resonant region. With the growth of energy $W_N > 2.3$ GeV the calculated cross section demonstrates a sharp increase associated with an insufficiently rapid attenuation of the hypertriton function obtained from the nonrelativistic equation (14) with an increase in energy.

In this work, systematic calculations of the cross sections of kaon photo- and electroproduction on the lightest nuclei d and ^{3}He are performed, taking into account the final state interaction. It is shown that the KN and YN interactions, indeed, turn out to be important in the threshold region for the kaon photo- and electroproduction on the deuteron. The contribution of the KN interaction can increase the prediction of the impulse approximation up to 2.5 times in the near-threshold region, and the combined contribution of the KN and YN interactions can increase σ_{IA} up to 4 times. At the same time, the available experimental data are not enough to unambiguously exclude one or another model of KN or YN interaction from consideration.

A procedure for finding the proper wave functions of three-body systems was developed and applied, that made it possible to find the functions of the ^{3}He and $^3_\Lambda$H nuclei. In contrast to the work of [8], the calculated hypertriton eigenfunction generates a bound state with a binding energy of $\approx$2.3 MeV. Calculations with these functions are in remarkable agreement with the available experimental data. It is shown that the main features of the cross sections of the processes under consideration are dictated by the structure of the elementary operator of photo- and electroproduction, as well as the eigenfunctions of the target nuclei. A correlation has been found in some kinematic regions between the wave function of ^{3}He and the contribution of final state interaction processes, which can be noticeable not only in the region of large kaon emission angles, where the contribution of the impulse approximation is minimal, but also in the small-angle region, where the contribution of the impulse approximation is decisive. The developed formalism of kaon electroproduction processes on light nuclei can be easily generalized to the processes of Σ-hypernuclei production, whose wave functions can also be directly found by solving Eq. (14) for the coupled ΣNN-ΛNN system.

VI. CONCLUSION

Calculations of the total and differential cross sections of kaon photo- and electroproduction on the deuteron in all charge channels, as well as kaon photo- and electroproduction in the processes of $^3\mathrm{He}(\gamma_V, K^+)^3_\Lambda\mathrm{H}$ and $^3\mathrm{He}(\gamma_V, K^+\Lambda)X$, were performed in this work. Calibration of the elementary photoproduction operator on a neutron was carried out according to the experimental data on quasifree $K^0\Lambda$ photoproduction on a deuteron. Calculations of the differential cross sections of the kaon electroproduction in various charge channels at $W_N = 1.91$ GeV and $Q^2 = 0.35$ GeV^2 show that the developed model agrees with the few experimental data in the region of small kaon emission angles already in the impulse approximation. The contributions of the final state interaction processes in the region of small kaon emission angles turned out to be negligible. The role of the final state interaction processes themselves is noticeable only in the region of large kaon emission angles in differential cross sections and in the near-threshold regions in total cross sections, respectively. The contribution of KN and YN final state interactions can increase the prediction of the impulse approximation up to several times in the near-threshold region of kaon photoproduction. However, the available experimental data are not enough to unambiguously exclude one or another model of KN or YN interaction from consideration.

For coherent and incoherent processes of kaon electroproduction on the ^{3}He nucleus the exact eigenfunctions of

the ^{3}He and $^3_\Lambda$H nuclei were obtained in this work. The calculations of the differential cross sections of kaon electroproduction on ^{3}He indicate a correlation between the used wave function of the target nucleus and the contribution of the final state interaction processes. Theoretical cross sections for $^3\mathrm{He}(\gamma_V, K^+)^3_\Lambda\mathrm{H}$ and $^3\mathrm{He}(\gamma_V, K^+\Lambda)X$ are also in a good agreement with the few available experimental data at the small kaon emission angles. One can also conclude that the available experimental data are not enough to unambiguously exclude one or another model of KN or YN interaction in the final state. Finally, this work demonstrates the first calculations of the total cross sections of kaon photoproduction in the processes $^3\mathrm{He}(\gamma, K^+)^3_\Lambda\mathrm{H}$ and $^3\mathrm{He}(\gamma, K^+\Lambda)X$.

ACKNOWLEDGMENTS

The work was funded by RFBR, Project No. 20-02-00004. Few-body quantum calculations were done under the Tomsk State University Development Programme (Priority-2030).

[1] N. Compton *et al.*, Measurement of the differential and total cross sections of the $\gamma d \to K^0\Lambda p$ reaction within the resonance region, Phys. Rev. C **96**, 065201 (2017).
[2] T. Mart, C. Bennhold, H. Haberzettl, and L. Titator, *Kaon-Maid 2000* (Institute für Kernphysik, Unversität Mainz, Germany, 2000).
[3] A. Anisovich, R. Beck, E. Klempt, V. Nikonov, A. Sarantsev, and U. Thoma, Properties of baryon resonances from a multichannel partial wave analysis, Eur. Phys. J. A **48**, 1 (2012).
[4] F. Dohrmann *et al.*, Angular Distribution for $^{3,4}_\Lambda$H Bound States in the $^{3,4}\mathrm{He}(e, e'K^+)$ Reaction, Phys. Rev. Lett. **93**, 242501 (2004).
[5] F. Dohrmann *et al.*, Quasifree Λ, Σ^0, and Σ^- electroproduction from ^{1,2}H, ^{3,4}He, and carbon, Phys. Rev. C **76**, 054004 (2007).
[6] T. Mart, L. Tiator, D. Drechsel, and C. Bennhold, Electromagnetic production of the hypertriton, Nucl. Phys. A **640**, 235 (1998).
[7] O. V. Maxwell, Photoproduction of kaons from ^{3}He, Phys. Rev. C **72**, 034601 (2005).
[8] T. Mart and B. I. S. van der Ventel, Photo- and electroproduction of the hypertriton on ^{3}He, Phys. Rev. C **78**, 014004 (2008).
[9] R. Nasseripour *et al.* (CLAS Collaboration), Coherent photoproduction of π^+ from ^{3}He, Phys. Rev. C **83**, 034001 (2011).
[10] S. Kamalov and L. Tiator, Two-Body Mechanisms in Pion Photoproduction on the Trinucleon, Phys. Rev. Lett. **75**, 1288 (1995).
[11] C. Dover and S. Yang, The $^3\mathrm{He}(\gamma, \pi^+)\,^3$H reaction in the (3, 3) resonance region, Phys. Lett. B **50**, 217 (1974).
[12] S. Costanza *et al.* (A2 Collaboration), Helicity dependence of the $\gamma^3\mathrm{He} \to \pi\mathrm{X}$ reactions in the $\Delta(1232)$ resonance region, Eur. Phys. J. A **50**, 173 (2014).
[13] B. Bellinghausen, H. Gassen, G. Nöldeke, E. Reese, T. Reichelt, P. Stipp, and H. Synal, Elastic photoproduction of charged pions on ^{3}He and ^{3}H in the $\Delta(1232)$ resonance region, Nucl. Phys. A **470**, 429 (1987).
[14] F. Pheron *et al.*, Coherent photoproduction of η-mesons off ^{3}He–search for η-mesic nuclei, Phys. Lett. B **709**, 21 (2012).
[15] L. Witthauer *et al.* (A2 Collaboration), Quasi-free photoproduction of η-mesons off ^{3}He nuclei, Eur. Phys. J. A **49**, 154 (2013).
[16] I. Keshelashvili, D. Werthmüller, and L. Witthauer, Quasi-free photoproduction of η-mesons off ^{2}H and ^{3}He, Int. J. Mod. Phys: Conf. Series **26**, 1460114 (2014).
[17] M. Egorov and V. Postnikov, Kaon electroproduction on the proton, J. Exp. Theor. Phys. **133**, 32 (2021).
[18] D. Skoupil and P. Bydžovský, Photoproduction of $K\Lambda$ on the proton, Phys. Rev. C **93**, 025204 (2016).
[19] M. Egorov, Coherent photoproduction of two neutral pseudoscalar mesons on light nuclei, Phys. Rev. C **101**, 065205 (2020).
[20] R. Machleidt, The bonn meson-exchange model for the nucleon-nucleon interaction, Phys. Rep. **149**, 1 (1987).
[21] V. Baru, J. Haidenbauer, C. Hanhart, and J. H. Niskanen, New parametrization of the trinucleon wave function and its application to the $\eta\,^3$He scattering lenth, Eur. Phys. J. A **16**, 437 (2003).
[22] W. Glöckle, *The Quantum Mechanical Few-Body Problem* (Springer-Verlag, Berlin, 1983), Chap. 3.
[23] M. Egorov, Kaon-hyperon-nuclear systems in the Faddeev approach (unpublished); see also preprint https://assets.researchsquare.com/files/rs-2021229/v1/covered.pdf?c=1664877594.
[24] J. Haidenbauer, Y. Koike, and W. Plessas, Separable representation of the Bonn nucleon-nucleon potential, Phys. Rev. C **33**, 439 (1986).
[25] M. Egorov and V. Postnikov, Integral equations and binding energies for Λ-NN, Λ-NNN systems, Nucl. Phys. A **1009**, 122172 (2021).
[26] N. Nagels, Th. A. Rijken, and Y. Yamamoto, Extended-soft-core baryon-baryon model ESC16 II. Hyperon-nucleon interactions, Phys. Rev. C **99**, 044003 (2019).
[27] Th. A. Rijken, Momentum-space Lippmann-Schwinger-equation. Fourier-transform with Gauss-expansion-method, arXiv:1409.5593.
[28] H. Bandō, T. Motoba, M. Sotona, and J. Žofka, Polarization of hypernuclei in the (π^+, K^+) reaction, Phys. Rev. C **39**, 587 (1989).
[29] H. Kamano, S. X. Nakamura, T.-S. H. Lee, and T. Sato, Dynamical coupled-channels model of K^-p reactions: determination of partial-wave amplitudes, Phys. Rev. C **90**, 065204 (2014).
[30] J. Révai and N. V. Shevchenko, Faddeev calculations of the $\bar{K}NN$ system with a chirally motivated $\bar{K}N$ interaction. II. The K^-pp quasibound state, Phys. Rev. C **90**, 034004 (2014).
[31] M. G. L. N. Santos and C. C. Barros, Jr., Low energy kaon-hyperon interaction, Phys. Rev. C **99**, 025206 (2019).
[32] S. Schneider, A. Sibirtsev, Ch. Elster, J. Haidenbauer, S. Krewald, and J. Speth, ηN final-state interaction in incoherent photoproduction of η-mesons from the deuteron, Eur. Phys. J. A **18**, 421 (2003).